Journal of Solid Mechanics Vol. 13, No. 3 (2021) pp. 297-304
DOI: 10.22034/jsm.2021.1879427.1502

Investigation of Stress State of the Layered Composite with a Longitudinal Cylindrical Cavity

V. Yu. Miroshnikov *

Department of Aircraft Strength of the National Aerospace University, Kharkov, Ukraine

Received 29 May 2021; accepted 5 July 2021

ABSTRACT

The article presents the study of the stress state of a two-layer composite with a cylindrical cavity located parallel to the surfaces of the layers. Displacements are set on the cavity and the upper and lower boundaries of the upper and lower layers, respectively. The three-dimensional elasticity solution has been obtained by the analytical-numerical generalized Fourier method with respect to the system of Lame equations in local cylindrical coordinates associated with cavity and Cartesian coordinates associated with boundaries of the layers. The infinite systems of linear algebraic equations resulting from satisfying the boundary conditions are solved by the reduction method. As a result, displacements and stresses have been obtained at various points of the elastic body. We have compared the stress-strain state of a two-layer structure with a cylindrical cavity located in either of the layers. The analysis included various geometrical parameters and boundary functions; the results obtained were compared with a single-layer holed structure.

Keywords: Composite; Cylindrical cavity in a layer; Generalized Fourier method; Bessel functions; Analytical and numerical methods.

1 INTRODUCTION

As the sintering technology of materials with different elastic characteristics develops [1], the need arises to study the stress state of such composites. Thus, laboratory tests are described in [2-4] choosing the most optimal arrangement options for layers and determining the mechanical properties of a particular composite. Another approach is analytical methods for simulating mechanical properties [5-7], which consider a composite made of isotropic layers as an integral transversely isotropic or orthotropic material, and its mechanical properties as functions of the layer thickness. Once the mechanical properties are determined, the problem for the layer is considered. In [8], two-layer metal sheets are investigated, where forming limit diagrams (FLDs) and forming limit stress diagrams (FLSDs) determined by analytical and numerical approaches are compared with experimental results of Al3105-St14 two-layer sheet to verify the validity of theoretical models. Many works are devoted to a composite layer or plate with a stress concentrator in the form of a cylindrical cavity perpendicular to the boundaries of the

*Corresponding author.Tel.: +38 067 7893333.
E-mail address: *v.miroshnikov@khai.edu* (V. Yu. Miroshnikov).

layer [9–12]. If we speak about the composite as an integral material, then its nonlinear mechanical behavior should be considered. The authors of [13] review rate-dependence, tension-compression asymmetry, viscous behavior, unloading characteristics, interaction between stress components and effects of environmental factors on mechanical properties. In this manuscript [14], the progressive failure analysis was employed to predict the final failure of notched woven glass/epoxy composite laminates under tensile loading. A user-defined material model (UMAT) in the Abaqus finite-element package was developed to utilize the 3D progressive failure analysis feasible. In the present manuscript [15], an extensive numerical study has been conducted to investigate the effects of material nonlinearity on the stress distribution and stress concentration factors in unidirectional and laminated composite materials. To achieve this objective, various models with different configurations were studied. In this manuscript [16], a comprehensive numerical analysis is conducted to assess the accuracy of the Tan's model of obtaining the stress concentration factor, for a plate with finite dimensions containing an open hole. The influence of plate length on the stress distribution around the hole is studied. The authors of [17] obtained the closed analytical expressions for the displacement field due to a cylindrical inclusion in a thermoelastic half-space. These expressions are derived in the context of steady-state uncoupled thermoelasticity using thermoelastic displacement potential functions.
The generalized Fourier method [18] is used to solve multiple boundary surface problems. Based on this method, problems have been solved for a half-space with longitudinal cylindrical cavities [19, 20], for a layer with a longitudinal cavity, insertions, or pipe [21-24]. Based on the generalized Fourier method, problems have also been solved for a cylinder with cylindrical cavities or insertions [25-28].

This paper suggests a solution to a spatial problem with a numerical-analytical approach based on the generalized Fourier method. The solution is recorded for each isotropic layer. The cylindrical cavity is located in one of the layers, provided that the boundary surfaces do not intersect. Consideration of the influence of boundary conditions on surfaces is based on addition theorems that connect the basic vector solutions of the Lame equation in Cartesian and cylindrical coordinates.

2 PROBLEM STATEMENT

There are two ideally sintered homogeneous elastic layers. The lower layer has a cylindrical cavity with radius R, parallel to its surfaces (Fig. 1).

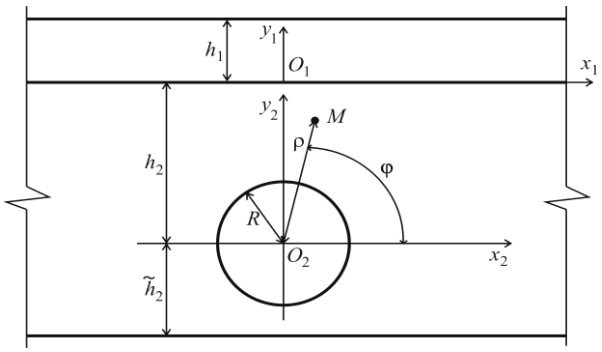

Fig.1
Two layers with a cylindrical cavity.

We shall consider the upper and lower layers in the Cartesian coordinate systems (x_1, y_1, z_1) and (x_2, y_2, z_2), respectively; the cavity will be considered in the cylindrical coordinate system (ρ, ϕ, z) aligned with the coordinate system of the lower layer. The boundaries of the upper and lower layers are located at the distance $y_1=h_1$ and $y_1=0$ and $y_2=h_2$ и $y_2=-\tilde{h}_2$, respectively.

We need to find a solution to the Lamé equation, where j is the layer number, provided that displacements are set at the upper boundary $y_1=h_1$ of the upper layer, at the lower boundary $\Delta\vec{U}_j+\left(1-2\sigma_j\right)^{-1}\nabla div\vec{U}_j=0$ of the lower layer and on the surface of the cavity $y_2=-\tilde{h}_2$:

$$\vec{U}_1\left(x_1,z_1\right)_{|y_1=h_1}=\vec{U}_1^0\left(x_1,z_1\right)\ ,\ \vec{U}_2\left(x_2,z_2\right)_{|y_2=-\tilde{h}_2}=\vec{U}_2^0\left(x_2,z_2\right)\ ,\ \vec{U}_2\left(\varphi,z\right)_{|\rho=R}=\vec{U}_R^0\left(\varphi,z\right)$$

where $\vec{U}_1$ are displacements in the upper layer; $\vec{U}_2$ are displacements in the lower layer;

$$\begin{aligned}
&\vec{U}_1^{\,0}\left(x_1,z_1\right)=U_x^{(1)}\vec{e}_1^{(1)}+U_y^{(1)}\vec{e}_2^{(1)}+U_z^{(1)}\vec{e}_3^{(1)}\ ,\\
&\vec{U}_2^{\,0}\left(x_2,z_2\right)=U_x^{(2)}\vec{e}_1^{(1)}+U_y^{(2)}\vec{e}_2^{(1)}+U_z^{(2)}\vec{e}_3^{(1)},\\
&\vec{U}_R^{\,0}\left(\varphi,z\right)=U_\rho^{(R)}\vec{e}_1^{(2)}+U_\varphi^{(R)}\vec{e}_2^{(2)}+U_z^{(R)}\vec{e}_3^{(2)}
\end{aligned}\tag{1}$$

Known functions; $\vec{e}_j^{(k)}$, j = 1, 2, 3 are the unit vectors of the Cartesian (k=1) and cylindrical (k=2) coordinate systems. The specified functions will be considered as rapidly decreasing from the origin along the z axis for the cylinder and along the z and x axes for the layer boundaries. The flat interface of the layers meets the boundary coupling conditions

$$\vec{U}_1\Big|_{y_1=0}=\vec{U}_2\Big|_{y_2=h_2}\tag{2}$$

$$F_1\vec{U}_1\Big|_{y_1=0}=F_2\vec{U}_2\Big|_{y_2=h_2}\tag{3}$$

where $F_j\,\vec{U}_j\Big|=2G_j[\dfrac{\sigma_j}{1-2\sigma_j}\vec{n}\,\mathrm{div}U_j+\dfrac{\partial}{\partial n}\vec{U}_j+\dfrac{1}{2}(\vec{n}\times rot\vec{U}_j)]$; $G_j=\dfrac{E_j}{2(1+\sigma_j)}$; σ_j, E_j are Poisson's ratio and modulus of elasticity of the *j-th* layer, respectively.

3 METHOD OF SOLUTION

Let us choose basic solutions for the Lamé equation for Cartesian and cylindrical coordinate systems in the form [18]:

$$\begin{aligned}
&\vec{u}_k^{\pm}\left(x,y,z;\lambda,\mu;\sigma\right)=N_k^{(d)}e^{i(\lambda z+\mu x)\pm\gamma y}\ ;\\
&\vec{R}_{k,m}\left(\rho,\varphi,z;\lambda;\sigma\right)=N_k^{(p)}I_m\left(\lambda\rho\right)e^{i(\lambda z+m\varphi)};\\
&\vec{S}_{k,m}\left(\rho,\varphi,z;\lambda;\sigma\right)=N_k^{(p)}\left[s_m\left(\rho;\lambda\right)\cdot e^{i(\lambda z+m\varphi)}\right];\qquad k=1,2,3;
\end{aligned}\tag{4}$$

$$\begin{aligned}
&N_1^{(d)}=\frac{1}{\lambda}\nabla;\ N_2^{(d)}=\frac{4}{\lambda}(\sigma-1)\vec{e}_2^{(1)}+\frac{1}{\lambda}\nabla(y\,\cdot);\ N_3^{(d)}=\frac{i}{\lambda}\mathrm{rot}\left(\vec{e}_3^{(1)}\cdot\right);\ N_1^{(p)}=\frac{1}{\lambda}\nabla;\\
&N_2^{(p)}=\frac{1}{\lambda}\left[\nabla\left(\rho\frac{\partial}{\partial\rho}\right)+4(\sigma-1)\left(\nabla-\vec{e}_3^{(2)}\frac{\partial}{\partial z}\right)\right];\ N_3^{(p)}=\frac{i}{\lambda}\mathrm{rot}\left(\vec{e}_3^{(2)}\cdot\right);\\
&s_m\left(\rho;\lambda\right)=\left(\mathrm{sign}\,\lambda\right)^m K_m\left(|\lambda|\rho\right);\ \gamma=\sqrt{\lambda^2+\mu^2},\ -\infty<\lambda,\mu<\infty,
\end{aligned}$$

where $I_m(x)$, $K_m(x)$ are modified Bessel functions; $\vec{R}_{k,m}$, $\vec{S}_{k,m}$ are internal and external solutions to the Lamé equation for the cylinder, respectively; $\vec{u}_k^{(-)}$, $\vec{u}_k^{(+)}$ are solutions to the Lamé equation for a layer.

The solution to the problem may be represented as:

$$\vec{U}_1=\sum_{k=1}^{3}\int_{-\infty}^{\infty}\int_{-\infty}^{\infty}\left(H_k^{(1)}\left(\lambda,\mu\right)\cdot\vec{u}_k^{(+)}\left(x_1,y_1,z_1;\lambda,\mu;\sigma_1\right)+\tilde{H}_k^{(1)}\left(\lambda,\mu\right)\cdot\vec{u}_k^{(-)}\left(x_1,y_1,z_1;\lambda,\mu;\sigma_1\right)\right)d\,\mu d\,\lambda\tag{5}$$

$$\vec{U}_2 = \sum_{k=1}^{3} \int_{-\infty}^{\infty} \sum_{m=-\infty}^{\infty} B_{k,m}(\lambda) \cdot \vec{S}_{k,m}(\rho,\varphi,z;\lambda;\sigma_2) d\lambda + \\ + \sum_{k=1}^{3} \int_{-\infty}^{\infty} \int_{-\infty}^{\infty} \left(H_k^{(2)}(\lambda,\mu) \cdot \vec{u}_k^{(+)}(x_2,y_2,z_2;\lambda,\mu;\sigma_2) + \tilde{H}_k^{(2)}(\lambda,\mu) \cdot \vec{u}_k^{(-)}(x_2,y_2,z_2;\lambda,\mu;\sigma_2) \right) d\mu d\lambda, \tag{6}$$

where $\vec{S}_{k,m}(\rho,\varphi,z;\lambda;\sigma_j)$, $\vec{u}_k^{(+)}(x,y,z;\lambda,\mu;\sigma_j)$ and $\vec{u}_k^{(-)}(x,y,z;\lambda,\mu;\sigma_j)$ are the basic solutions, which are given by formulas (4), and the unknown functions $H_k^{(1)}(\lambda,\mu)$, $\tilde{H}_k^{(1)}(\lambda,\mu)$, $H_k^{(2)}(\lambda,\mu)$, $\tilde{H}_k^{(2)}(\lambda,\mu)$ and $B_{k,m}(\lambda)$ and must be found from the boundary conditions (1).

To make the transition of basic solutions between coordinate systems (Fig. 1), we use the formulas [24]. To satisfy the boundary conditions at the upper boundary of the upper layer, we equate vector (5) ($y_1=h_1$) to the specified $\vec{U}_1^0(x_1,z_1)$, represented through the double Fourier integral. Thus, we get the first three equations (one for each projection) with six unknowns $H_k^{(1)}(\lambda,\mu)$, $\tilde{H}_k^{(1)}(\lambda,\mu)$.

To satisfy the boundary conditions at the lower boundary of the lower layer, we rewrite the vectors $\vec{S}_{k,m}$ in (6), using the transition formulas [24, formula 7], in the Cartesian coordinate system through the basic solutions $\vec{u}_k^{(+)}$. Then we equate the resulting vector ($y_2=-\tilde{h}_2$) to the specified $\vec{U}_2^0(x_2,z_2)$, represented through the double Fourier integral.

Considering that the vector of displacements for the lower boundary of the upper layer is equal to the vector of displacements of the upper boundary of the lower layer, we can write three additional equations in the form (2). In this case, writing down the expression $\vec{U}_2(x_2,z_2)_{|y_2=h_2}$, we shall use the formulas for the transition from solutions $\vec{S}_{k,m}$ of the cylinder to solutions $\vec{u}_k^{(-)}$ [24, formula 7]. Similarly, we can write three additional equations for stresses (3). As a result, we obtain a system of 12 equations and use them to express the functions $H_k^{(1)}(\lambda,\mu)$, $\tilde{H}_k^{(1)}(\lambda,\mu)$, $H_k^{(2)}(\lambda,\mu)$, $\tilde{H}_k^{(2)}(\lambda,\mu)$ though $B_{k,m}(\lambda)$.

The determinant Δ of this system has the form $\Delta = \dfrac{64 \cdot \gamma^7 \cdot e^{-6\gamma h_1} \cdot \Phi(\gamma)}{\lambda^4}$, where $\Phi(\gamma)$ is a function, which is omitted due to its cumbersomeness. The study $\Phi(\gamma)$ showed that, if $\gamma > 0$, it has only positive values and does not vanish. Given that $\Delta > 0$, this system of equations has a unique solution.

To satisfy the boundary conditions at the cylinder $\rho = R$, we rewrite the right side [6] using the transition formulas from solutions $\vec{u}_k^{(+)}$ to solutions $\vec{u}_k^{(-)}$ [24, formula 8], in the Cartesian coordinate system through the basic solutions $\vec{R}_{k,m}$, $\vec{S}_{k,m}$. Then we equate the resulting vector to the specified $\vec{U}_R^0(\varphi,z)$, represented through the integral and the Fourier series. As a result, we obtain a set of three infinite systems of linear algebraic equations to find unknowns. These infinite systems have the properties of equations of the second kind, which makes them possible to apply the reduction method. Once $B_{k,m}(\lambda)$ is determined, we can find the unknowns $H_k^{(1)}(\lambda,\mu)$, $\tilde{H}_k^{(1)}(\lambda,\mu)$, $H_k^{(2)}(\lambda,\mu)$, $\tilde{H}_k^{(2)}(\lambda,\mu)$, which had been expressed through $B_{k,m}(\lambda)$. Similarly, we will find all unknown expressions (5) and (6).

4 NUMERICAL STUDIES OF THE STRESS STSTE

The cylindrical cavity is located in the lower layer of a two-layer isotropic material (Fig. 1). Physical characteristics of the upper layer: Poisson's ratio σ_1 = 0.21, elastic modulus E_1 = 294000 *N/mm*^{2}; lower layer: σ_2 = 0.38, E_2 = 1700

N/mm^2. The radius of the cylindrical cavity is $R = 10mm$. Thickness of the upper layer $h_1 = 4mm$, thickness of the lower layer $h_2 + \tilde{h}_2 = 60mm$. Distance to the cylindrical cavity was calculated in triplicate: for $h_2 = 30mm$, $h_2 = 40mm$, and $h_2 = 20mm$. For comparison, the option without the upper layer was taken. On the surface of the cylinder, we set displacements $U_\rho^{(R)}(\varphi, z) = 10^4 \cdot \left(z^2 + 10^2\right)^{-2}$, $U_\varphi^{(R)} = U_z^{(R)} = 0$, on the upper boundary of the upper layer and the lower boundary of the lower layer, respectively.

The infinite system was truncated by the parameter m. $h_2 = 30mm$, $m = 6$; $h_2 = 40mm$ and $h_2 = 20mm$ with $m = 9$. The integrals were calculated using the Philon quadrature formulas (for oscillating functions) and Simpson (for zero oscillation functions). The accuracy of meeting the boundary conditions, with the specified m and geometric parameters, is 10^{-3}.

Fig. 2 presents the stresses σ_ρ and $\tau_{\rho z}$ at the boundary of the layers along the z axis, $\varphi = \pi/2$. The stress curves σ_φ and σ_z have the same form as they differ only in maximum values $\sigma_\rho = \sigma_\varphi$ = –18.59 *MPa*, $h_2 = 30mm$, $\sigma_z = \sigma_\varphi$ = –73.13 *MPa*, $h_2 = 20mm$, and $\sigma_z = \sigma_\varphi$ = –7.74 *MPa* at $h_2 = 40mm$.

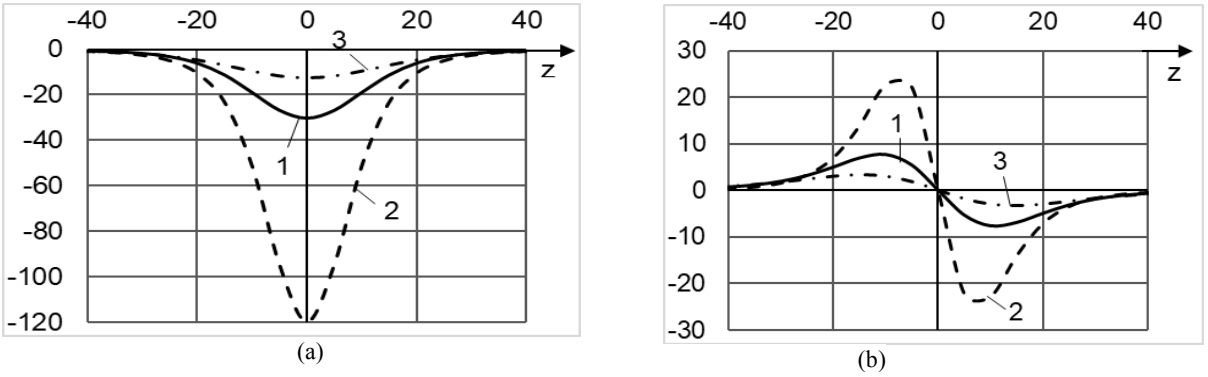

(a) (b)

Fig.2

Stresses at the boundary of layers, *MPa*: *a* – σ_ρ; *b*– $\tau_{\rho z}$; 1 – $h_2 = 30mm$, 2 – $h_2 = 20mm$, 3 – $h_2 = 40mm$.

Fig. 2 shows the growing stresses at the boundary of the layers as the hole approaches the upper layer (line 2) and their decrease as the hole moves away (line 3). The absence of the upper layer has little effect on the stress state of the upper boundary of the lower layer (changes less than 1%) and are omitted on the curve due to the coincidence of the lines.

Fig.3 shows the stresses σ_ρ and $\tau_{\rho\varphi}$ on the surface of the cylindrical cavity, z=0. The stress curves σ_φ and σ_z have the same form as they differ only in σ_ρ, ranging from 3.58 to 54.83 *MPa*, and σ_φ, ranging from –67.84 to –119.65 *MPa*.

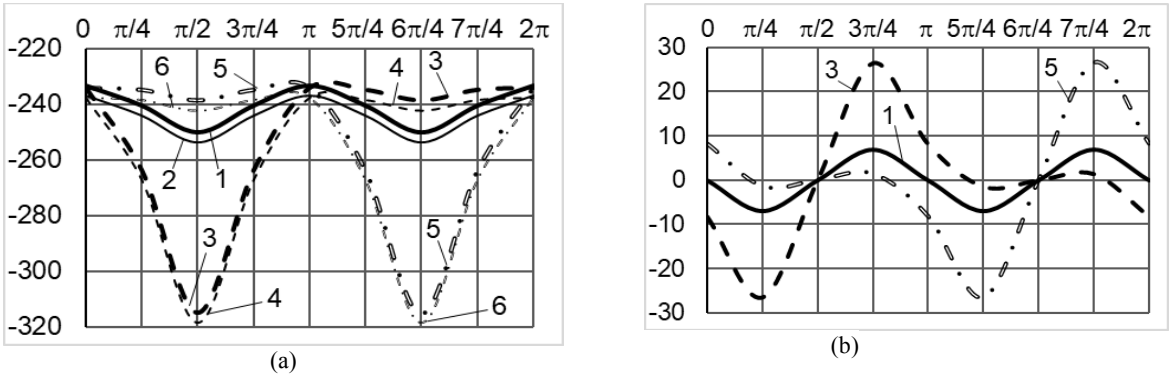

(a) (b)

Fig.3

Stresses on the surface of the cylindrical cavity, *MPa*: *a* – σ_ρ; *b* – $\tau_{\rho\varphi}$; 1 – $h_2 = 30mm$; 2 – $h_2 = 30mm$, without upper layer; 3 – $h_2 = 20mm$; 4 – $h_2 = 20mm$, without upper layer; 5 – $h_2 = 40mm$; 6 – $h_2 = 40mm$, without upper layer.

Curves in Fig. 3 show the greater stresses on the surface of the cylindrical hole on the closer side to one of the layer boundaries. If $h_2 = 20mm$, the stress is higher at $\pi/2$ (lines 3, 4), if $h_2 = 40mm$, the stress is higher at $6\pi/4$ (lines 5, 6), if $h_2 = 30mm$, symmetry is observed (lines 1, 2). The absence of the upper layer causes an increase in stresses σ_ρ, σ_φ, σ_z on the surface of the cavity (Fig. 3(a), lines 2, 4, 6), while the shear stresses $\tau_{\rho\varphi}$ (Fig. 3(b)) remain practically unaffected.

If we change the functions of the boundary conditions and set zero displacements $U_\rho^{(R)} = U_\varphi^{(R)} = U_z^{(R)} = 0$ on the surface of the cylinder, $U_y^{(1)}(\varphi, z) = -10^8 \cdot \left(z^2 + 10^2\right)^{-2} \cdot \left(x^2 + 10^2\right)^{-2}$ and $U_x^{(1)} = U_z^{(1)} = 0$ at the upper boundary of the upper layer, and $U_x^{(2)} = U_y^{(2)} = U_z^{(2)} = 0$ at the lower boundary of the lower layer, then the nature of the stress state will change.

For such boundary conditions, Fig. 4 shows the stresses σ_ρ, σ_φ, σ_z and $\tau_{\rho z}$ at the boundary between the layers (in the lower layer body) along the z axis.

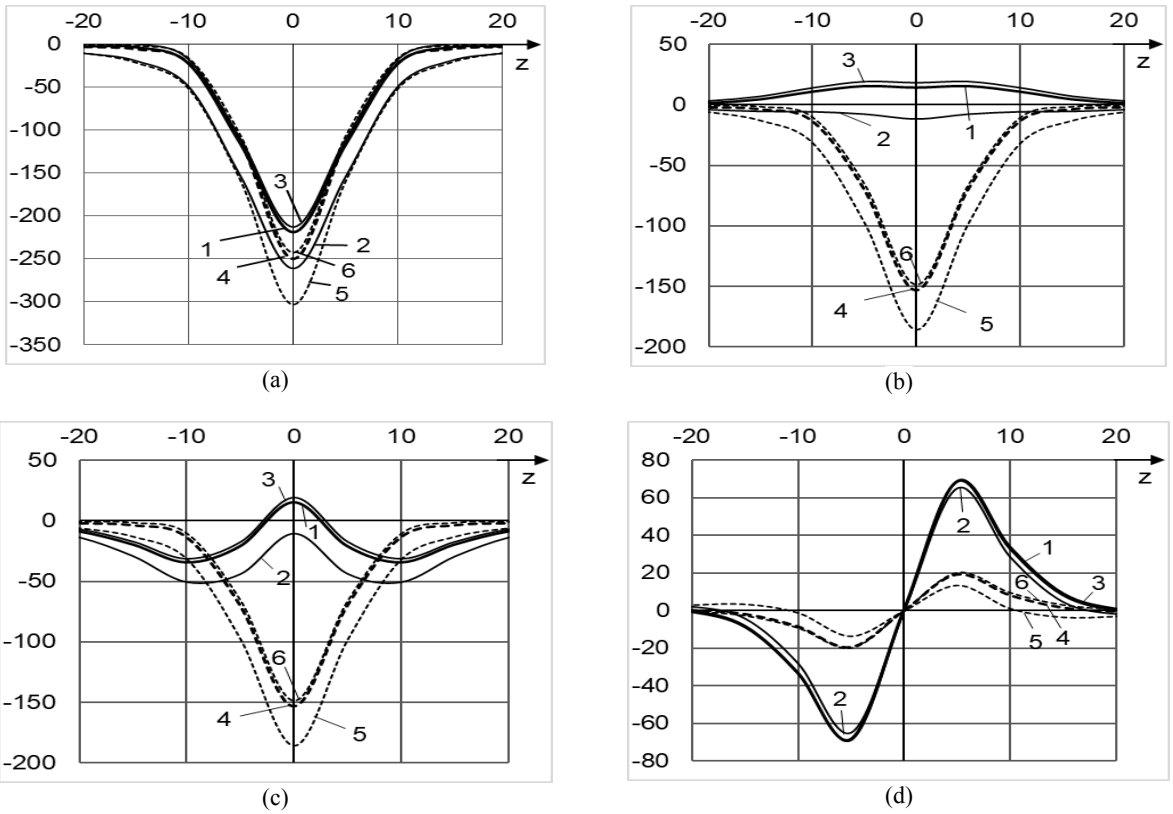

Fig.4

Stresses between the layers, *MPa*: $a - \sigma_\rho$; $b - \sigma_\varphi$, $c - \sigma_z$, $d - \tau_{\rho z}$; 1 – $h_2 = 30mm$; 2 – $h_2 = 30mm$, without upper layer; 3 – $h_2 = 20mm$; 4 – $h_2 = 20mm$, without upper layer; 5 – $h_2 = 40mm$; 6 – $h_2 = 40mm$, without upper layer.

Stresses σ_ρ at the boundary between the layers (Fig. 4(a)) increase as the hole approaches this boundary (line 2). A significant increase is also caused by the absence of the upper layer (nonzero displacements in this case are applied to the upper boundary of the lower layer), thus, line 1 (Fig. 4(a)) passes into line 4, line 2 passes into line 5, and line 3 passes into line 6. Stresses σ_φ at the boundary between the layers (Fig. 4(b)) at $h_2 = 30mm$ and $h_2 = 40mm$ (lines 1 and 3, respectively) have positive values; as the hole approaches this boundary ($h_2 = 20mm$, line 2), the values become negative. In the absence of the upper layer, all stresses σ_φ become negative and grow significant: line 1 (Fig. 4(b)) passes into line 4, line 2 passes into line 5, and line 3 passes into line 6. The forms of stress curves σ_z at the boundary between the layers (Fig. 4(c)) with (lines 1, 2, 3) and without an upper layer (lines

4, 5, 6) differ significantly. In the presence of the upper layer, the stress σ_z is significantly lower; moreover, if $h_2 = 30mm$ and $h_2 = 40mm$ (lines 1 and 3, respectively) the stresses in the region $z = 0$ have positive values. Shear stresses $\tau_{\rho z}$ (Fig. 4(d)), in the presence of the upper layer, have greater values (lines 1, 2, 3) than without it (lines 4, 5, 6). The height of the hole location has little effect on the values of shear stresses $\tau_{\rho z}$; moreover, if $h_2 = 30mm$ and $h_2 = 40mm$ (lines 1 and 3, respectively), they practically coincide.

On the surface of the cylinder, at $z = 0$, stresses σ_ρ and $\tau_{\rho\varphi}$ are shown in Fig. 5. The stress values on the lower part of the cylindrical cavity (angle $\varphi = \pi \ldots 2\pi$) are close to zero and are omitted in Fig. 5. The stress curves σ_φ and σ_z have the same form as σ_ρ ; the only different values are the maximum values in the presence of the upper layer $\sigma_\varphi = -18.37\ MPa$, $\sigma_z = -18.45\ MPa$ at $h_2 = 30mm$, $\sigma_\varphi = -66.45\ MPa$, $\sigma_z = -66,5\ MPa$ at $h_2 = 20mm$, and $\sigma_\varphi = \sigma_z = -7.88\ MPa$ at $h_2 = 40mm$.

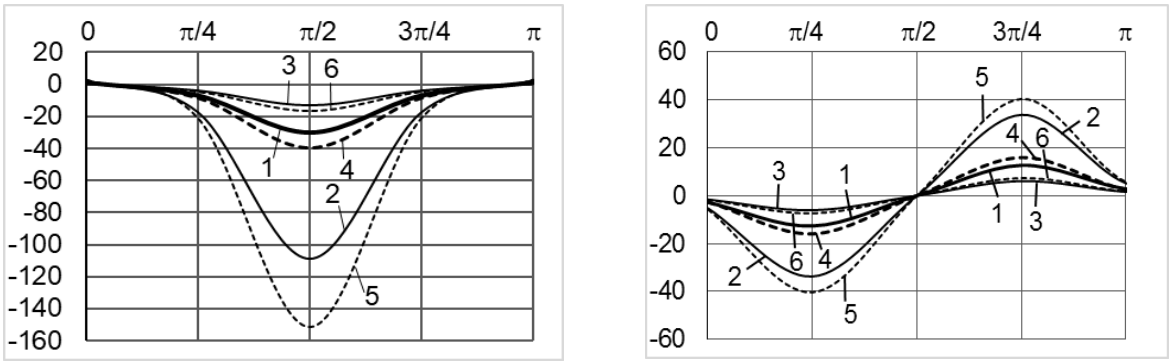

(a) (b)

Fig.5

Stresses on the surface of the cylindrical cavity, *MPa*: $a - \sigma_\rho$; $b - \tau_{\rho\varphi}$; 1 – $h_2 = 30mm$; 2 – $h_2 = 30mm$, without upper layer; 3 – $h_2 = 20mm$; 4 – $h_2 = 20mm$, without upper layer; 5 – $h_2 = 40mm$; 6 – $h_2 = 40mm$, without upper layer.

In the absence of the upper layer (Fig. 5, lines 4, 5, 6), the stress is higher than with it (Fig. 5, lines 1, 2, 3); thus, line 1 passes into line 4, line 2 passes into line 5, and line 3 passes into line 6. As the cavity approaches the upper boundary of the layer, the stresses increase (lines 2 and 5).

5 CONCLUSION

We have proposed a method for solving the second main three-dimensional elasticity problem on the basis of the generalized Fourier method for two heavily bonded layers with a cylindrical cavity in either of them. The problem is reduced to an infinite system of linear algebraic equations, which allows applying the truncation method. Numerical studies give grounds to say that the proposed method can help find its solution with any accuracy, which is confirmed by the high accuracy of fulfilling the boundary conditions. The solution method can be applied in the design of composites, with two bonded layers with a cylindrical cavity and boundary conditions in the form of displacements used as a design model. The presented comparative analysis shows the influence of the upper (protective) layer and the cylindrical cavity on the stress state of the lower (main) layer having a stress concentrator. This analysis can be used to select the geometric parameters of the structure.

REFERENCES

[1] Vityaz P. A., Kovaliova S. A., Zornik V. I., Kukareko V.A., Grigorieva T. F., Gamzeleva T. V., Lyakhov N. Z., 2012, Structure and tribological properties of cu-sn alloys based on mechanical activated powders formed by electro contact sintering, *The Eleventh Israeli-Russian Bi-National Workshop 2012 ,The Optimization of the Composition, Structure and Properties of Metals, Oxides, Composites, Nano and Amorphous Materials* **2012**: 181-190.

[2] Aitharaju V., Aashat S., Kia H., Satyanarayana A., Bogert P., 2016, Progressive damage modeling of notched composites, *NASA Technical Reports Server*.
[3] Ershova A. Yu., Martirosov M. I., 2014, Experimental studies of polymer composites with fine filler (tensile-compression tests), *Structural Mechanics of Engineering Structures and Structures* **5**: 61-69.
[4] Hu J., Zhang K., Cheng H., Liu P., Zou P., Song D., 2017, Stress analysis and damage evolution in individual plies of notched composite laminates subjected to in-plane loads, *Chinese Journal of Aeronautics* **30**(1): 447-460.
[5] Pelekh B. L., Makhnitskii R. N., 1981, Approximate methods for solving problems on the concentration of stresses around apertures in Orthotropic disks made out of composite materials, *Mechanics of Composite Materials* **16**(6): 690-693.
[6] Pobedrya B. E., Gorbachev V. I., 1984, Stress and strain concentration in composite materials, *Mechanics of Composite Materials* **20**(2): 141-148.
[7] Annin B. D., Maksimenko V. N., 1989, Evaluation of the failure of plates made of composite materials with holes, *Mechanics of Composite Materials* **25**(2): 216-222.
[8] Deilami Azodi H., Darabi R., 2017, Theoretical, numerical and experimental investigation on formability of Al3105-St14 two-layer sheet, *Journal of Solid Mechanics* **9**(2): 434-444.
[9] Ghasemi A.R., Razavian I., 2012, Measurement of variation in fracture strength and calculation of stress concentration factor in composite laminates with circular hole, *Journal of Solid Mechanics* **4**(3): 226-236.
[10] Jafari M., Bayati Chaleshtari M. H., Ardalani E., 2018, Determination of optimal parameters for finite plates with a quasi-square hole, *Journal of Solid Mechanics* **10**(2): 300-314.
[11] Dastjerdi Sh., Yazdanparast L., 2018, New method for large deflection analysis of an elliptic plate weakened by an eccentric circular hole, *Journal of Solid Mechanics* **10**(3): 561-570.
[12] Abolghasemi S., Eipakchi H.R., Shariati M., 2018, Investigation of pre-buckling stress effect on buckling load determination of finite rectangular plates with circular cutout, *Journal of Solid Mechanics* **10**(4): 816-830.
[13] Fallahi H., Taheri-Behrooz F., Asadi A., 2020, Nonlinear mechanical response of polymer matrix composites: A review, *Polymer Reviews* **60**(1): 42-85.
[14] Taheri-Behrooz F., Bakhshan H., 2018, Characteristic length determination of notched woven composites, *Advanced Composite Materials* **27**(1): 67-83.
[15] Taheri-Behrooz F., Bakhshi N., 2017, Neuber's rule accounting for the material nonlinearity influence on the stress concentration of the laminated composites, *Journal of Reinforced Plastics and Composites* **36** (3): 214-225.
[16] Bakhshi N., Taheri-Behrooz F., 2019, Length effect on the stress concentration factor of a perforated orthotropic composite plate under in-plane loading, *International Journal* **of** *Composite* **Materials 1**: 71-90.
[17] Singh K., Renu M., 2017, Displacement field due to a cylindrical inclusion in a thermoelastic half-space, *Journal of Solid Mechanics* **9**(3): 445-455.
[18] Nikolaev A. G., Protsenko V. S., 2011, *A Generalized Fourier Method in Spatial Problems of the Theory of Elasticity*, Kharkov, National Aerospace University.
[19] Miroshnikov V. Yu., 2018, First basic elasticity theory problem in a half-space with several parallel round cylindrical cavities, *Journal of Mechanical Engineering* **21**(2): 12-18.
[20] Protsenko V., Miroshnikov V., 2018, Investigating a problem from the theory of elasticity for a half-space with cylindrical cavities for which boundary conditions of contact type are assigned, *Eastern-European Journal of Enterprise Technologies Applied mechanics* **4**(94): 43- 50.
[21] Miroshnikov V. Yu., 2019, The study of the second main problem of the theory of elasticity for a layer with a cylindrical cavity, *Strength of Materials and Theory of Structures* **102**: 77-90.
[22] Miroshnikov V. Yu., 2020, Stress state of an elastic layer with a cylindrical cavity on a rigid foundation, *International Applied Mechanics* **56**(3): 372-381.
[23] Miroshnikov V. Yu., Medvedeva A. V., Oleshkevich S. V., 2019, Determination of the stress state of the layer with a cylindrical elastic inclusion, *Materials Science Forum* **968**: 413-420.
[24] Miroshnikov V., 2019, Investigation of the stress strain state of the layer with a longitudinal cylindrical thick-ealled tube and the displacements given at the boundaries of the layer, *Journal of Mechanical Engineering* **22**(2): 44-52.
[25] Nikolaev A. G., Tanchik E. A., 2016, Stresses in an elastic cylinder with cylindrical cavities forming a hexagonal structure, *Journal of Applied Mechanics and Technical Physics* **57**(6): 1141-1149.
[26] Nikolaev A. G., Tanchik E. A., 2016, Model of the stress state of a unidirectional composite with cylindrical fibers forming a tetragonal structure, *Mechanics of Composite Materials* **52**(2): 177-188.
[27] Nikolaev A. G., Tanchik E. A., 2015, The first boundary-value problem of the elasticity theory for a cylinder with N cylindrical cavities, *Numerical Analysis and Applications* **8**: 148-158.
[28] Nikolaev A. G., Tanchik E. A., 2016, Stresses in an infinite circular cylinder with four cylindrical cavities, *Journal of Mathematical Sciences* **217**(3): 299-311.